Arch Appl Mech (2010) 80: 503–512
DOI 10.1007/s00419-009-0380-4

SPECIAL ISSUE

André Lutz · Udo Nackenhorst

Numerical investigations on the biomechanical compatibility of hip-joint endoprostheses

Received: 21 October 2008 / Accepted: 1 October 2009 / Published online: 20 October 2009

Abstract A computational approach for studies on the biomechanical compatibility of hip implants based on detailed three-dimensional finite element models is presented. With the anticipation for a meaningful computational prediction of bone behavior under endoprosthetic treatment a general modeling approach taking into account the model generation from radiological data and the recovery of statically equivalent joint loads and muscle forces from a best fit between simulated and measured bone mass density distribution was developed. Computational results for three different endoprostheses systems are presented and compared with clinical studies. The potential for aiding the development process of new prosthesis designs regarding their biomechanical compatibility is demonstrated.

Keywords Stress adaptive bone remodeling · Hip-joint endoprosthetics · Finite element method

1 Introduction

Artificial joint replacement is one standard surgery for joint diseases. With more than 100,000 implantations per year hip-joint endoprosthetics is the most frequent treatment in Germany. A typical complication is aseptic loosening of the implant-bone integration with the indication for revision. Stress shielding caused by unphysiological load transfer due to the stiff implant is discussed as one major source for these failure scenario. Besides the requirement on the biocompatibility of the implanted materials, investigations on optimized prosthesis designs with better biomechanical compatibility are performed. Computational mechanics can assist to accelerate these developments.

Since Wolff [1] stated his law of bone-transformation in the late nineteenth century the relation between bone formation and mechanical demand is well accepted. Pioneering work in this field has also been done by Pauwels [2]. Starting with the late 1980s going along with increased computer performance and related development of computational mechanics first theories on stress adaptive bone remodeling have been developed [3–7], which have been refined for more and more sophisticated analysis in the following years; among many others here it is referred to [8] for early computational aspects and to [9–12] for recent constitutive approaches within a continuum mechanics framework. Nowadays a couple of advanced theories for the constitutive modeling of stress driven bone remodeling phenomena are available, considering anisotropic behavior

A. Lutz (✉) · U. Nackenhorst
Institute of Mechanics and Computational Mechanics, Leibniz Universität Hannover,
Appelstraße 9a, 30167 Hannover, Germany
E-mail: lutz@ibnm.uni-hannover.de
Tel.: +49-511-762-2286

U. Nackenhorst
E-mail: nackenhorst@ibnm.uni-hannover.de
Tel.: +49-511-762-3560
Fax: +49-511-762-19053

as well as large deformation response [9,10,12] or two-phase approaches considering the liquid phase of bone tissue [13].

Current developments mainly focus on the improvement of rather specific issues, like more sophisticated constitutive formulations. But so far, a strong link between the mechanical stimulation of bone remodeling as long temporal term response at the continuum level and the responsible cells activity is an open field of research. While the signaling process between the sensor cells (osteocytes) and bone remodeling cells (osteoclasts and osteoblasts) appears to be understood [14], the physiological environment for the stimulation of cell activities remains under controversy discussions [15–17]. Thus the mechanical stimulus assumptions provided within a continuum mechanics description have a strong heuristic character. In contrast, but closely related to the former statement, there is only a limited knowledge about the individual mechanical loading conditions of the bone due to muscle forces and joint loads at all. Besides the fact, that this issue has already been addressed in the early publications on stress adaptive bone remodeling, e.g. [3,6], only limited improvement has been recognized by the authors. Data from experiments [18] regarding resultant hip joint forces and theoretical investigations for related muscle activities [19,20] are available. However, these knowledge is not processable for bone remodeling simulations directly, because an accumulation of a long motion history has to be taken into account.

Besides the mentioned uncertainties it appears hard to evaluate the constitutive parameters from related laboratory tests and it is almost impossible to validate these models from in vivo studies with current radiologic diagnostic tools. Till now it is only possible to explain the models plausibility based on clinical studies. Under these circumstances a hierarchical modeling approach appears to be suitable, starting with quite simple approaches regarding the constitutive description to study effects of predominant meaning. Once first order effects and dependencies are well understood, model refinements can start goal oriented for the most sensitive parameters.

A balanced modeling scheme will be presented in Sect. 2, where we restrict ourself to a quite simple mechanical approach (linear elasticity, isotropic material behavior, etc.). The geometry is reconstructed from CT-data from which also the initial bone mass density distribution is assigned to the finite element model. Based on this initial configuration statically equivalent loads set for joint forces and muscle loads are computed by an inverse approach ending up in a biomechanically equilibrated model for the physiological bone. For studies on the bone remodeling behavior of different hip-joint endoprosthesis designs a CAD model is reconstructed from the triangularized surface model which enables the intersection with the prosthesis geometries. The capability of the suggested modeling approach will be demonstrated for three different types of hip-joint endoprosthesis. A clear correspondence with clinical results will be shown. As a first step for model refinement a bioactive contact layer between prosthesis and bone will be introduced for simulation of the osseointegration of the non-cemented implants.

2 Modeling approach

The overall modeling approach for studies on the biomechanical compatibility of artificial hip joint replacements consists of different modeling steps. In the following the mathematical model for internal stress adaptive bone remodeling based on continuum mechanics is briefly outlined, followed by the geometrical modeling approach and an recovery technique for the computation of statically equivalent joint loads and muscle forces. As a first step for model refinement a bioactive contact layer will be introduced in between prosthesis shaft and bone for the simulation of osseointegration of implants.

2.1 Mathematical model for stress adaptive bone remodeling

For the computation of the mechanical stress distribution the local equilibrium condition

$$\operatorname{div} \boldsymbol{\sigma} = \mathbf{0} \tag{1}$$

for vanishing body forces ($\boldsymbol{b} = \mathbf{0}$) is solved. The Cauchy stress tensor $\boldsymbol{\sigma}$ is associated to a free energy density function such that

$$\boldsymbol{\sigma} = \varrho \frac{\psi}{\partial \boldsymbol{\varepsilon}} \tag{2}$$

with the linear strain tensor $\boldsymbol{\varepsilon} = \mathrm{sym}(\mathrm{grad}\ \boldsymbol{u})$, while $\boldsymbol{u}$ describes the displacement field. The free energy density function itself depends on the strain tensor and a set of internal variables $\boldsymbol{\alpha}$ which describe the load history of the material,

$$\psi = \psi(\boldsymbol{\varepsilon}, \boldsymbol{\alpha}). \tag{3}$$

By this first order approach isotropic and linear elastic constitutive behavior of bone tissue is assumed (see discussions below), and therefore a scalar valued internal variable associated to the macroscopic observable bone mass density (BMD) $\alpha \sim \varrho$ is introduced. With these assumptions the free energy density function takes the form

$$\psi = \frac{1}{2\varrho}\boldsymbol{\varepsilon} \cdot \cdot \boldsymbol{C}(\varrho) \cdot \cdot \boldsymbol{\varepsilon} \tag{4}$$

with the linear elastic fourth order constitutive tensor $\boldsymbol{C}$, which depends on the BMD only. Within the outlined model framework the constitutive tensor can expressed as

$$\boldsymbol{C} = \frac{E(\varrho)}{E_0}\boldsymbol{C}_0 \tag{5}$$

where $E(\varrho)$ describes the Youngs modulus of bone tissue in dependence of BMD, E_0 is a corresponding reference value, e.g. for cortical bone, and correspondingly $\boldsymbol{C}_0$ is a constant isotropic linear elastic constitutive tensor. Within a consistent framework of constitutive theory of materials, regarding which it is referred to monographs like [21] and related computation aspects to [22,23], a physiological target function is stated,

$$f = \psi - \psi_{\mathrm{phy}} = 0 \tag{6}$$

where ψ_{phy} describes a physiological target value, i.e. a long-time averaged strain energy state assumed to be comfortable for the living bone tissue from the macroscopic point of view. In close analogy to continuum damage mechanics from the postulate of extreme values of internal dissipation an evolution rule for the internal variables is derived,

$$\dot{\varrho} = \dot{\lambda}\frac{\partial f}{\partial \varrho}. \tag{7}$$

The numerical treatment within this generalized framework is well investigated, i.e. the equilibrium conditions are solved with finite element methods while the evolution equations for the internal variables are integrated locally with implicit Euler-schemes.

An open question remains on the constitutive relationship discussed for Eq. 5. Often cited is the empirical equation after Carter and Hayes [24],

$$E(\varrho) = 3790\ \dot{\varepsilon}^{0.06}\varrho^3, \tag{8}$$

who found from experiments with cortical human and bovine bone a cubic relationship between Youngs-modulus and apparent bone mass density. Besides these findings a lot of experimental investigations for cortical as well as trabecular bone for different anatomical locations are reported in literature, e.g. [25–30], linear regression as well as power laws like Eq. 8 are presented, while the exponent varies between $n = 1$ and $n = 3.3$. A systematic study comparing finite element results from six different relationships with experiments has been published in [31], who showed that by the Carter Hayes equation ($n = 3$) the computed strains appear overestimated while for example the approach after Morgan et al. ($n = 1.83$) appears to stiff.

From a theoretical analysis based on a thermodynamic consistent continuum mechanics constitutive theory Krstin et al. [10] argued a value for the exponent of $n = 2$. This is also in agreement with statistical analysis published in [32]. We found that the constitutive relation

$$E = E_0\left(\frac{\varrho}{\varrho_0}\right)^2 \tag{9}$$

with $E_0 = 6250$ MPa and $\varrho_0 = 1$ g/cm^3 provides a good fit to the findings of [31].

Remark on the constitutive approach. More sophisticated constitutive models for stress adaptive bone remodeling have been reported in literature including anisotropic or large deformation assumptions, here it is referred

to [9–12] for example. We decided for the outlined first order approach because of a lot of additional model uncertainties discussed below, and in this context the problem of model parameter identification. A setting within a large deformation continuum framework appears not suitable in bone mechanics (fracture stretch of about 1%) as far as no growth associated with anatomical shape changes is considered. Among others, e.g. [33,34], we made the experience that anisotropic effects appear of second order importance at least for the proximal femur region.

Remark on computational stability. In the early literature the phenomenon of checkerboarding has been discussed, e.g. [6,8], which appears with low order finite elements. For linear tetrahedral elements used for this investigations this problem is circumvented by smoothing the internal variable field using superconvergent patch recovery techniques described in [35] for example.

An other issue is on the often cited dead zone for the evolution of the bone mass rate equations, see e.g. [4,36]. From continuum constitutive theory there are no arguments for such non-smooth approaches, and from computational point of view sophisticated techniques have to be involved for the development of robust and stable algorithms.

2.2 Geometrical modeling and finite element discretization

The anatomical shape of the femur is reconstructed from computer tomography data available from the visible human project [37]. In a first step the outer geometry is reconstructed by using the segmentation techniques provided by Matlab-software, see Fig. 1a. For the purpose of virtual implantation of artificial joint endoprosthesis a CAD-reconstruction based on a smoothed triangularized surface model shown in Fig. 1b is performed. Using automated Delauny techniques the geometry is discretized with linear tetrahedral finite elements (Fig. 1c). The total mesh consists of about 15,000 linear tetrahedral elements resulting into approximately 3,500 unknown nodal displacements. Finally, as shown in Fig. 1d, the Hounsfield units identified from the CT-data are translated into BMD-values, for details it is referred to [38] for example, and mapped to the finite elements as initial values for the distribution of Youngs-moduli using Eq. 9.

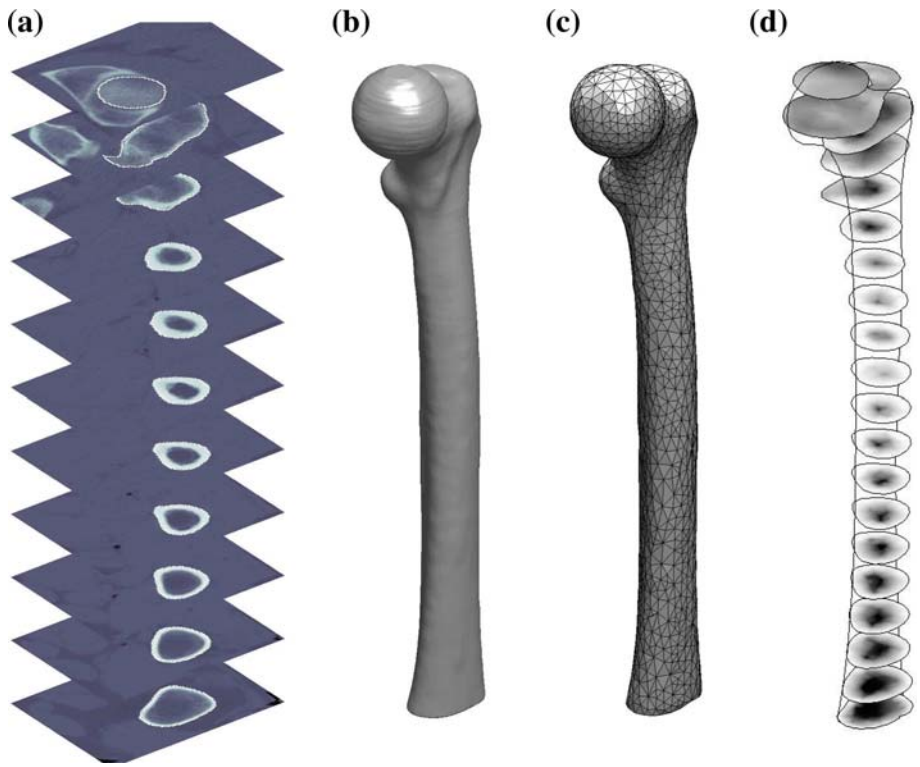

Fig. 1 Model generation process. From CT data (**a**) over a triangle surface model (**b**) to a tetrahedral finite element model (**c**) with mapped bone mass densities (**d**)

Once a biomechanical equilibrated model is obtained as discussed in the next subsection, a prosthesis model is easily integrated using CAD-techniques. This enables for studies of bone remodeling caused from different prosthesis design for assessing the biomechanical compatibility, see Sect. 3.

2.3 Boundary conditions and loads

For the computation of the equilibrium equations boundary conditions have to be defined. To suppress rigid body motions the femur model is kinematically restrained at its distal part. The shaft is modeled about 25-cm long, which is approximately 60% of the whole femur, so that local disturbances from Dirichlet conditions are dyed out. The femur is loaded by joint forces and nine muscle groups as depicted in Fig. 2. An inverse optimization approach is applied to compute a static equivalent load set: Based on the BMD-distribution obtained from the CT-data the joint forces and muscle loads are computed such that the remodeling algorithm leads to a BMD-distribution which fits best to the measured one. A similar technique has been already mentioned in [39]. The computed statically equivalent load set is collected in Fig. 2, from which it is observed that at least five muscle groups have to be considered for the proximal part of the femur.

Once the statical equivalent load set is found, a biomechanically equilibrated model of the femur is obtained which is the basis for studies on the stress adaptive bone remodeling caused by artificial joint implants, as discussed below.

2.4 Model refinement: bioactive contact interface

The modeling approach described before assumes a perfect bonding between bone and endoprosthesis because matching meshes with the same interface nodes are used. The surface of modern prosthesis shafts are functionally graded, where the osseointegration shall be enhanced by structured surfaces or bioactive coating for specific parts, while for other parts an ingrowths is avoided by polished surfaces. For that purpose a bioactive interface layer has been implemented. In a first step the contact interface nodes are doubled and an offset of 0.5 mm is generated. The obtained gap is filled with addition triangular wedge elements with contact specific constitutive properties (only normal pressure and related limited tangential shear is supported), see Fig. 3a. This is valid for all parts of the prosthesis, and for the textured and bioactive coated parts an ingrowth scenario depending on the mechanical environment is modeled. An outline of details is beyond the scope of this presentation, the basic features are that:

- large relative tangential displacements caused from dynamic short term loads prevent osseointegration locally
- ingrowth appears only at regions with predominant contact pressure
- the osseointegration occurs at much shorter time scales as bone remodeling (because of other cell activities) and therefore, appears finished before the overall bone remodeling simulation starts.

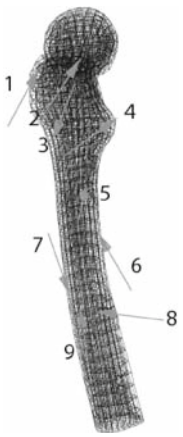

no.	muscle	F_x	F_y	F_z	F_R
	joint force	-952.93	-529.03	832.34	1371
2	gluteus medius	144.47	152.43	-172.47	272
1	gluteus minimus	363.97	274.36	-372.80	589
3	vastus lateralis	13.08	-63.02	123.79	139
4	psoas major. illiacus	38.25	190.03	-107.97	222
8	biceps fem., caput breve	-0.47	-20.33	-4.56	21
5	glueteus maximus	222.83	0.08	-21.07	223
7	vastus intermedialis	-2.60	11.48	56.49	58
9	vastus medialis	-0.42	0.00	-6.95	7
6	adductor longus	0.21	-1.68	-3.99	4

Fig. 2 Primary muscle forces after [40]

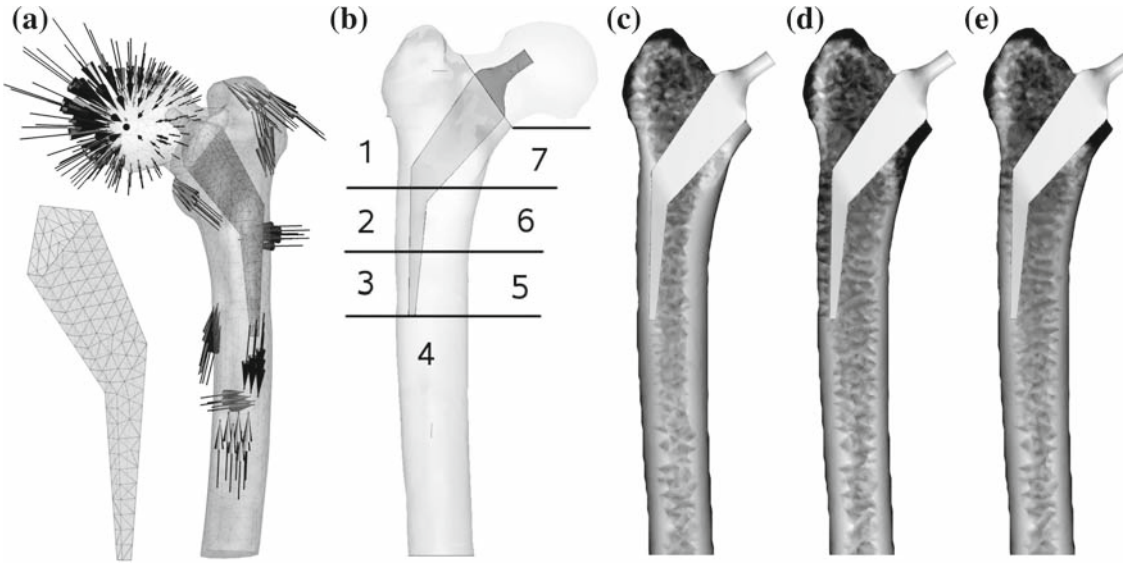

Fig. 3 Mayo FE-Model with loads and wedge contact layer magnified (**a**), Gruen zones (**b**), X-ray emulation of 3D bone apparent density distribution in postoperative state (**c**) and in longterm state without (**d**) and with contact elements (**e**)

3 A comparison of three hip-joint endoprosthesis

As first device the Mayo prostheses (Zimmer, Germany) has been analyzed. It is a short stem titanium implant with conical shaped rhombic cross section developed in the early 1980s and implanted since 1985. With this special design multi-point anchoring has been intended. The proximal part has a structured surface for osseointegration, while the distal tip is polished. The goal of this implant was to create a non-cemented short stem providing minimal bone loss, immediate fixation, long-term compatibility regarding good remodeling properties and the possibility of easy revision.

The finite element model depicted in Fig. 3a consists of about 4,300 nodes and nearly 20,000 linear tetrahedral elements. The model is fixed at its distal end and the joint force as well as the muscle forces are distributed as depicted in Fig. 3a for more physiologic loading by avoiding stress singularities. For comparison, this model has been simulated with both approaches, perfect bonding of the bone implant interface and the bioactive contact interface layer using 3-D wedge contact elements. The material properties of titanium, which are applied for this and the following implants are $E = 105.000$ MPa and $\nu = 0.31$.

Results of the finite element simulation are depicted in Fig. 3c–e for the postoperative state and for the long term state without and with contact elements in a X-ray emulation of the 3-D BMD distribution. The model with perfect bonding in the bone implant interface predicts massive stress shielding in Gruen zones (see Fig. 3b) 2, 3 and 7 and moderate atrophy in zone 1. This approach appears not suitable for this device, as the distal part of the implant is not fixed, but swinging freely. The model with contact elements provides much better results, as considerable atrophy is only predicted in zones 2 and 7, which is in good agreement with clinical studies. For example, Roth et al. [41] published a study with 8 patients in a mean age of 54.4 years. They performed DEXA measurements and got a mean BMD loss of $\approx$15% in zone 7 twelve months postoperatively. In zones 1, 2 and 3 the change in BMD was $\approx -5\%$, $\approx +3\%$ and $\approx -2\%$. In zones 4, 5 and 6 there was almost no change in BMD. The computation clearly underline these tendencies, while only in Gruen zone 2 the resorption appears overestimated.

Another study based on radiological follow-ups of 159 hips at a mean of 6.2 years postoperatively has been reported by Morrey et al. [42]. They recorded visible neocortex (divergent from the implant) in 27.5% of the patients in zone 1 and 2 and radiolucent lines in 13.8% of the patients again in zone 1 and 2. Neocortex visibility occurs 3.3 times more often in zone 1 compared to zone 2 and lucent lines are two times more often in zone 1. This is a indicator for atrophy in these zones. In the other zones these effects occurred only isolated. These clinical results are also in good agreement with the computational remodeling prediction.

Unfortunately, no quantitative data regarding the total loss of bone mass, e.g. from DEXA measurements, are available so far. With reference to discretized finite element volume a loss of bone mass of about 20% is predicted from the computed results for this device when the advanced contact theory has been considered.

As a second implant analyzed is the famous Zweymüller prosthesis has been analyzed. This titanium prosthesis has been introduced in 1979 and appears to be the most frequently implanted non-cemented stem-prosthesis in Europe. It was designed to provide primary rotation-safe stability due to press fit along the whole length of the implant [43]. The finite element model used for these investigations consists of about 15,100 linear tetrahedral elements with 3,200 nodes. To match the original design goals of this implant a perfect bonding along the whole stem has been modeled.

The computed results are depicted in Fig. 4b and c in postoperative and longterm state again as X-ray emulation. The corresponding Gruen zones are plotted in Fig. 4a. Due to the simulated perfect press fit fixation, stress shielding is evident in all Gruen zones except zone 4, whereas the accompanying bone loss decreases in distal direction. These results correlate quite good with radiological investigations of Effenberger et al. [44] for patients that encounter bone loss. Hanebeck [45] did a study with 95 patients and follow-ups after 2, 4 and 6 years. The radiologic follow-ups were attended by 29 (2 years), 29 (4 years) and 23 (6 years) patients. Atrophy was reported in the Gruen zones as summarized in Table 1. Most often atrophy is reported in proximal zones 1 and 7 and in moderate occurrence in zones 2 and 6. The study of Zwartele et al. [46] reveals similar results. They found bone atrophy in the majority of the femora predominantly in zones 1 and 7 (no quantitative information). In 22% of 142 femora bone atrophy was detected in three Gruen zones or more. So atrophy is more frequent in proximal parts and getting less in distal direction.

These findings are in clear correspondence with our computational results, while the loss of bone mass in Gruen zones 2 and 6 appears overestimated. This is the result of the perfect bonding assumption, the use of bioactive contact elements as in the former example might lead to better agreement with radiological observations regarding the overestimation of bone-loss in zones 2 and 6. It is assumed that the perfect press fit as it is simulated would not be achieved clinically and is, as the results show, not desirable. But as cases are described in literature, in which this stress-shielding behavior is reported, these results can be interpreted as worst case scenario.

The simulation predicts a total change of bone mass of 29%. So with ideal press fit fixation this implant tends to have higher-than-average stress-shielding behavior. Due to its long stem, its diaphyseal fixation and the accompanying diaphyseal load application to the bone this implant should be emphasized as revision implant rather than as primary device, particularly regarding younger patients with a high risk of revision.

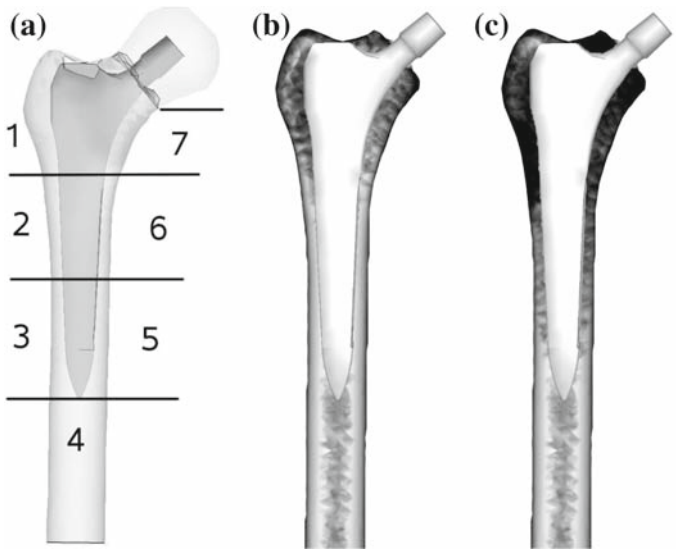

Fig. 4 Gruen zones (**a**) and X-Ray emulation of bone apparent density distribution in postoperative (**b**) and longterm state (**c**) of the Zweymüller prosthesis model

Table 1 Atrophy in the Gruen zones for three stages of follow-up in % of appearance in patients [45]

Follow-up	Gruen 1 (%)	Gruen 2 (%)	Gruen 3 (%)	Gruen 4 (%)	Gruen 5 (%)	Gruen 6 (%)	Gruen 7 (%)
2 years	55	21	0	0	0	14	41
4 years	55	17	7	0	0	7	34
6 years	52	30	9	0	0	14	39

Especially for younger patients attempts on preservative treatment are under investigation to ensure a rather good remaining bone stock in the proximal femoral region for revisions. A method for rather low resections is the resurfacing technique. A CAD model for a resurfacing cap prosthesis with femur is depicted in Fig. 5a, the corresponding finite element model consists of 45,000 linear tetrahedra with about 9,000 nodes.

The results of postoperative (Fig. 5b) and longterm state (Fig. 5c) are again compared in emulated X-ray graphics. There are almost no changes visible. Bone-loss only occurs directly under the cap, as the comparison of postoperative (Fig. 5d) and longterm (Fig. 5e) frontal cuts in the density distribution reveal. As the load is transferred from the cap to the cortical regions in the femur neck, no bone-loss occurs and the proximal bone stock remains. Quite good survival rates are reported in clinical studies (e.g. [47]), but in a significant number of cases complications like femoral neck fractures or loosening of the implant are reported. Falez et al. [48] report that there were neither clinical nor radiographic signs that indicated the fractures in their study. Examination of three failed specimens revealed necrosis in the epiphysis that extended to the femoral neck and caused one fracture and two times loosening of the implant. Another specimen showed extensive resorption of the femoral epiphysis. These diagnoses have been associated with massive cement penetration into the epiphyseal bone and polar cement concentration under the cap. Accompanying an interruption of the blood supply could lead to avascular necrosis followed by loosening of the implant [49]. Little et al. [50] found histological signs of avascular necrosis in 92% of cases, which were revised due to aseptic loosening or femoral neck fracture.

From pure mechanical point of view this kind of treatment appears preferable, but additional biomedical aspects have to be considered. With a loss of bone mass of only 6.2%, the hip joint resurfacing treatment is best regarding the remodeling abilities and the conservation of bone stock.

4 Conclusions

A first order computational approach for preclinical analysis of the biomechanical compatibility of hip-joint endoprosthesis has been outlined. The biological reaction of bones due to changes in mechanical demand has been described by a quite simple phenomenological model within a thermodynamically consistent constitutive framework. For these studies the model assumptions have been chosen as simple as possible, i.e. isotropic linear elastic constitutive behavior of bone tissue and a scalar valued internal variable for the evolution of the bone mass density in close analogy to continuum damage mechanics. The simplicity of this approach is argued as follows: Besides the constitutive relations there are a lot of other uncertainties, where the definition of the loading conditions are assumed to be predominantly. It appears to be impossible to obtain reliable constitutive parameters even for this simple model, the prognosis capability of the model can only be underlined by clinical studies. In addition, efficient numerical techniques for the stable and reliable solution of related problems are well established. The main focus of the current presentation is led onto a consistent overall modeling approach where the geometry and initial bone mass density distribution is recovered from CT-images. This initial model serves for the computation of statically equivalent load sets using an inverse simulation approach. As a first step for model refinement a bioactive contact layer for the prediction of the osseointegration of the implants has been introduced.

Based on this biomechanical equilibrated model of the human femur studies on the bone loss caused from three different hip-joint endoprostheses systems have been performed. The computational results have been compared with clinical data reported in literature. The computational prediction is in good agreement with radiological observation.

The studies presented here demonstrate illustratively, that even with this quite simple, but numerical efficient remodeling approach, the prior effects of stress adaptive bone remodeling are well described. From the

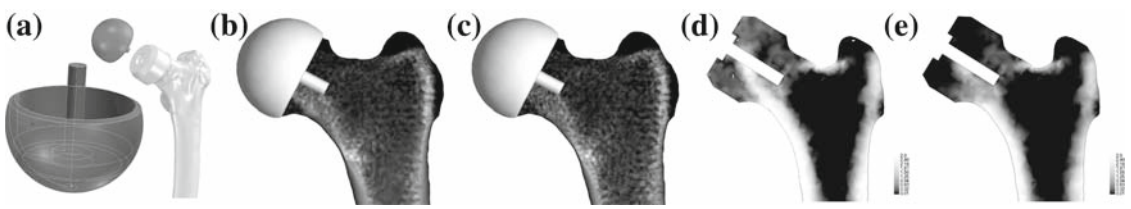

Fig. 5 CAD model of resurfacing implant and femur (**a**). X-ray emulation of density distribution in Mayo model in postoperative (**b**) and longterm state (**c**). Density distribution in frontal cuts in postoperative (**d**) and longterm state (**e**)

experience of the authors the results are much more sensitive on the loading conditions than on second order effects like anisotropy, etc. It has been outlined that a qualitative judgment of the biomechanical compatibility of bone implants is possible jet now, which might assist in the design of better prosthesis as well as patient individual therapy.

References

1. Wolff, J.: Das Gesetz der Transformationder Knochen. Hirschwald, Berlin (1892)
2. Pauwels, F.: Atlas zur Biomechanik der gesunden und kranken Hüfte. Springer, Berlin (1973)
3. Carter, D.R., Orr, T.E., Fyhrie, D.P.: Relationship between loading history and femoral cancellous bone architechture. J. Biomech. **22**, 231–244 (1989)
4. Beaupre, G.S., Orr, T.E., Carter, D.R.: An approach for time-dependent bone modeling and remodeling—theoretical development. J. Orthop. Res. **8**, 651–661 (1990)
5. Beaupre, G.S., Orr, T.E., Carter, D.R.: An approach for time-dependent bone modelling and remodelling: a preliminary remodeling simulation. J. Orthop. Res. **8**, 662–670 (1990)
6. Weinans, H., Huiskes, R., Grootenboer, H.J.: The behavior of adaptive bone remodeling simulation models. J. Biomech. **25**, 1425–1441 (1992)
7. Nackenhorst, U.: Numerical simulation of stress stimulated bone remodeling. Technische Mechanik **17**, 31–40 (1997)
8. Jacobs, C.R., Levenston, M.E., Beaupre, G.S., Simo, J.C., Carter, D.R.: Numerical instabilities in bone-remodeling simulations: the advantage of a node-based finite element approach. J. Biomech. **28**, 449–459 (1995)
9. Jacobs, C.R., Simo, J.C., Beaupre, G.S., Carter, D.R.: Adaptive bone remodeling incorporating simultaneous density and anisotropy considerations. J. Biomech. **30**, 603–613 (1997)
10. Krstin, N., Nackenhorst, U., Lammering, R.: Zur konstitutiven Beschreibung des anisotropen beanspruchungsadaptiven Knochenumbaus. Technische Mechanik **20**, 31–40 (2000)
11. Doblare, M., Garcia, J.M.: Anisotropic bone remodelling model based on a continuum damage–repair theory. J. Biomech. **35**, 1–17 (2002)
12. Kuhl, E., Menzel, A., Steinmann, P.: Computational modeling of growth—A critical review, a classification of concepts and two new consistent approaches. Comput. Mech. **32**, 71–88 (2003)
13. Cowin, S.C., Hegedus, D.H.: Bone remodeling. I. Theory of adaptive elasticity. J. Elast. **6**, 313–326 (1976)
14. Cowin, S.C.: Bone Mechanics Handbook. CRC Press, Boca Raton (2001)
15. Martin, R.B.: Is all cortical bone remodeling initiated by microdamage? Bone **30**, 8–13 (2002)
16. You, L., Cowin, S.C., Schaffler, M.B., Weinbaum, S.: A model for strain amplification in the actin cytoskeleton of osteocytes due to fluid drag on pericellular matrix. J. Biomech. **34**, 1375–1386 (2001)
17. MacGinitie, L.A., Stanley, G.D., Bieber, W.A., Wu, D.D.: Bone streaming potentials and currents depend on anatomical structure and loading orientation. J. Biomech. **30**, 1133–1139 (1997)
18. Bergmann, G., Deuretzbacher, G., Heller, M., Graichen, F., Rohlmann, A., Strauss, J., Duda, G.N.: Hip contact forces and gaint pattern from routine activities. J. Biomech. **34**, 859–871 (2001)
19. Heller, M.O., Bergmann, G., Kassi, J.P., Claes, L., Haas, N.P., Duda, G.N.: Determination of muscle loading at the hip joint for use in pre-clinical testing. J. Biomech. **38**, 1155–1163 (2005)
20. Duda, G., Heller, M., Bergmann, G.: Musculosceletal loading database: loading conditions of the proximal femur. Theor. Issues Ergon. Sci. **6**, 287–292 (2005)
21. Lemaitre, J., Chaboche, J.-L.: Mechanics of Solid Materials. Cambridge University Press, Cambridge (1990)
22. Simo, J.C., Hughes, T.J.R.: Computational Inelasticity. Springer, Berlin (1998)
23. Wriggers, P.: Nonlinear Finite Element Methods. Springer, Berlin (2008)
24. Carter, D.R., Hayes, W.C.: The behavior of bone as a two-phase porous structure. J. Bone Joint Surg. **59**, 954–962 (1977)
25. Linde, F., Norgaard, P., Hvid, I., Odgaard, A., Soballe, K.: Mechanical properties of trabecular bone: dependency on strain rate. J. Biomech. **24**, 803–809 (1991)
26. Cody, D., Hou, F.J., Divine, G.W., Fyhrie, D.P.: Short term in vivo precision of proximal femoral finite element modeling. Ann. Biomed. Eng. **28**, 408–414 (2000)
27. Keyak, J.H., Falkinstein, Y.: Comparison of in situ and in vitro CT scan-based finite element model predictions of proximal femoral fracture load. Med. Eng. Phys. **25**, 781–787 (2003)
28. Snyder, S.M., Schneider, E.: Estimation of mechanical properties of cortical bone by computed tomography. J. Orthop. Res. **9**, 422–431 (1991)
29. Wirtz, D.C., Schiffers, N., Pandorf, T., Radermacher, K., Weichert, D., Forst, R.: Critical evaluation of known bone material properties to realize anisotropic FE-simulation of the proximal femur. J. Biomech. **33**, 1325–1330 (2000)
30. Rho, J.Y., Hobatho, M.C., Ashman, R.B.: Relations of mechanical properties to density and CT numbers in human bone. Med. Eng. Phys. **17**, 347–355 (1995)
31. Austmann, R.L., Milner, J.S., Holdsworth, D.W., Dunning, C.E.: The effect on the density-modulus relationship selected to apply material properties in a finite element model of long bone. J. Biomech. **41**, 3171–3176 (2008)
32. Rice, J.C., Cowin, S.C., Bowman, J.A.: On the dependence of elasticity and strength of cancellous bone on apparent density. J. Biomech. **21**, 155–168 (1988)
33. Peng, L., Bai, J., Zeng, X., Zhou, Y.: Comparison of isotropic and orthotropic material property assignments on femoral finite element models under two loading conditions. Med. Eng. Phys. **28**, 227–233 (2006)
34. Baca, V., Horak, Z., Mikulenka, P., Dzupa, V.: Comparison of an inhomogeneous orthotropic and isotropic material models used for FE analyses. Med. Eng. Phys. **30**, 924–930 (2008)
35. Zienkiewicz, O.C., Zhu, J.Z.: The superconvergence patch recovery and a posteriori error estimates. Part I. The recovery techniques. Int. J. Numer. Methods Eng. **33**, 1331–1364 (1992)

36. Weinans, H., Huiskes, R., Verdonschot, B., Van Rietbergen, N.: The effect of adaptive bone remodeling threshold levels on resoprtion around noncemented hip stems. Adv. Bioeng. **20**, 303–306 (1991)
37. National Library of Medicine. Visible Human Project. 08 July 2009. http://www.nlm.nih.gov/research/visible/visible_human.html
38. Yosibash, Z., Padan, R., Joskowicz, L., Milgrom, C.: A CT-based high-order finite element analysis of the human proximal femur compared to in vitro experiments. J. Biomech. Eng. **129**, 297–309 (2007)
39. Fischer, K.J., Jacobs, C.R., Carter, D.R.: Computational method for determination of bone and joints loads using bone density distributions. J. Biomech. **28**, 1127–1135 (1995)
40. Ebbecke, B., Nackenhorst, U.: Simulation of stress adaptive bone remodeling. J. Struct. Mech. **38**, 177–180 (2005)
41. Roth, A., Richartz, G., Sander, K., Sachse, A., Fuhrmann, R., Wagner, A., Venbrocks, R.A.: Verlauf der periprothetischen Knochendichte nach Hüfttotalendoprothesenimplantation. Orthopäde **34**, 334–344 (2005)
42. Morrey, B.F., Adams, R.A., Kessler, M.: A conservative femoral replacement for total hip arthroplasty—a prospective study. J. Bone Joint Surg. **82**, 952–958 (2000)
43. Zweymüller, K., Lintner, F., Semlitsch, M.: Biologic fixation of a press-fit titanium hip joint endoprosthesis. Clin. Orthop. Relat. Res. **235**, 195–206 (1988)
44. Effenberger, H., Ramsauer, T., Böm, G., Hilzensauer, G., Dorn, U., Lintner, F.: Successful hip arthroplasty using cementless titanium implants in rheumatoid arthritis. Arch. Orthop. Trauma Surg. **122**, 80–87 (2001)
45. Hanebeck, J.: Postoperative Knochendichteänderungen am Femur nach Implantation der zementfreien Zweymüller-Hüft-endoprothese unter Berücksichtigung klinischer und röntgenologischer Parameter. PhD Thesis, Humbold Universität Berlin (2001)
46. Zwartele, R., Peters, A., Brouwers, J., Olsthoorn, P., Brand, R., Doets, C.: Long-term results of cementless primary total hip arthroplasty with a threaded cup and a tapered, rectangular titanium stem in rheumatoid arthritis and osteoarthritis. Int. Orthop. **32**, 581–587 (2008)
47. Daniel, J., Pynsent, P.B., McMinn, D.J.: Metal-on-metal resurfacing of the hip in patients under the age of 55 years with osteoarthritis. J. Bone Joint Surg. Br. **86**, 177–184 (2004)
48. Falez, F., Favetti, F., Casella, F., Panegrossi, G.: Hip resurfacing: why does it fail? Early results and critical analysis of our first 60 cases. Int. Orthop. **32**, 209–216 (2007)
49. Lavigne, M., Kalhor, M., Beck, M., Ganz, R., Leunig, M.: Distribution of vascular foramina around the femoral head and neck junction: relevance for conservative intracapsular procedures of the hip. Orthop. Clin. North Am. **36**, 171–176 (2005)
50. Little, C.P., Ruiz, A.L., Harding, I.J., McLardy-Smith, P., Gundle, R., Murray, D.W., Athanasou, N.A.: Osteonecrosis in retrieved femoral heads after failed resurfacing arthroplasty of the hip. J. Bone Joint Surg. Br. **87**, 320–323 (2005)